The Effects of Ultrasound Pressure and Temperature Fields in Millisecond Bubble Nucleation

Matheus Oliveira de Andrade[a], Seyyed Reza Haqshenas[a], Ki Joo Pahk[b], Nader Saffari[a]

[a] UCL Mechanical Engineering, University College London, London, WC1E 7JE, United Kingdom; [b] Center for Bionics, Biomedical Research Institute, Korea Institute of Science and Technology (KIST), Seoul, 02792, Republic of Korea

Keywords: Bubble Nucleation; HIFU; Histotripsy; Cavitation; Boiling.

Declaration of interest: none.

Corresponding author: M. O. de Andrade <matheus.andrade.15@ucl.ac.uk>

Abstract

A phenomenological implementation of Classical Nucleation Theory (CNT) is employed to investigate the connection between high intensity focused ultrasound (HIFU) pressure and temperature fields with the energetic requirements of bubble nucleation. As a case study, boiling histotripsy in tissue-mimicking phantoms is modelled. The physics of key components in the implementation of CNT in HIFU conditions such as the derivation of nucleation pressure thresholds and approximations regarding the surface tension of the liquid are reviewed and discussed. Simulations show that the acoustic pressure is the ultimate trigger for millisecond bubble nucleation in boiling histotripsy, however, HIFU heat deposition facilitates nucleation by lowering nucleation pressure thresholds. Nucleation thus occurs preferentially at the regions of highest heat deposition within the HIFU field. This implies that bubble nucleation subsequent to millisecond HIFU heat deposition can take place at temperatures below 100 °C as long as the focal HIFU peak negative pressure exceeds the temperature-dependent nucleation threshold. It is also found that the magnitude of nucleation pressure thresholds decreases with decreasing frequencies. Overall, results indicate that it is not possible to separate thermal and mechanical effects of HIFU in the nucleation of bubbles for timescales of a few milliseconds. This

methodology provides a promising framework for studying time and space dependencies of the energetics of bubble nucleation within a HIFU field.

1. Introduction

In recent years, an important shift in perspective has changed the way that cavitation is regarded in biomedical ultrasound. Bubble activity induced by high intensity focused ultrasound has been shown to cause repeatable mechanical disintegration of soft-tissue [1,2]. This method is termed histotripsy, where the growth and violent collapse of vapour/gas bubbles fragments soft tissue into subcellular debris. Histotripsy has found potential applications for the treatment of benign prostatic hyperplasia (BPH), liver and kidney tumours, enhancement of anti-tumour immune response, tissue decellularisation and cell therapy [2,3].

Consequently, some research activity has shifted from designing protocols free from bubble activity [4-7] to those which will take advantage of its bioeffects to perform non-invasive tissue disintegration [2]. There are two traditional modes for the initiation of bubbles in histotripsy: cavitation-cloud histotripsy (CCH) [8,9], and boiling histotripsy (BH) [10,11]. Both approaches use periodic pulses of ultrasound irradiation, but differ in pulse duration and pulse repetition frequency (PRF).

In boiling histotripsy, pulse durations are usually of the order of 10 – 20 ms and low PRFs are employed. The pulse duration is *n* cycles at the source frequency, and the PRF is the number of pulses delivered per second. Non-linear propagation effects distort the acoustic waves, resulting in the formation of shocks at the HIFU focus. The higher harmonics in these shockwaves are readily absorbed by the medium, causing intense heat deposition until a vapour bubble is created at high temperatures. Conversely, in cavitation-cloud histotripsy, the pulse durations are shorter (1 μs – 1 ms), but delivered more frequently. This ensures that no significant heat deposition happens so that bubble nucleation is caused exclusively by the ultrasound tensile pressures or by the interaction of incoming waves and those reflected from possible pre-existing bubbles. When bubble nucleation can be repeatedly obtained with short ultrasound pulses, histotripsy is referred to as intrinsic histotripsy [2].

The extent of mechanical damage in histotripsy lesions has been argued to depend ultimately on the mechanical properties of the target tissue subjected to bubble activity [12,13]. This places histotripsy as a potential form of controlled, self-limiting therapy whose destructive action depends on the structural properties of tissue and the

onset of cavitation. However, a significant drawback in the clinical use of ultrasound-induced cavitation relates to the highly uncertain character of bubble nucleation in acoustic fields [14]. Such uncertainty could arguably have been responsible for the slower development and clinical application of ultrasonic therapies that use bubble activity compared to those only using thermal effects. Currently, most Food and Drug Administration (FDA) approved modes of ultrasound therapy use thermal modes of HIFU only [14]. Indeed, the controlled nucleation of bubbles in living tissue has been regarded as one of the central challenges in the biomedical applications of ultrasound [15,16].

Research into vapour-phase nucleation and bubble activity in water has mostly involved simulations of bubble dynamics [17-19]. This methodology relies on the assumption that stabilised gas pockets nucleate spontaneously at some time before HIFU sonication and survive in body fluids [20,21]. The main issue with this hypothesis is the very slim chances of survival of unstabilised microbubbles in such media. Gas bubbles in liquids tend to dissolve away due to Laplace pressure in the absence of a stabilising force [20-24]. Furthermore, assuming the existence of stabilised bubbles in soft-tissue also proposes that the content of body fluids is comparable to that of untreated water systems. In untreated water systems, preferential nucleation sites are normally hydrophobic crevices where gas is trapped or free-flowing gas bubbles [23,25]. However, review of a number of studies concluded that no hydrophobic crevices had ever been observed in tissues or capillaries [23].

Despite the availability of sophisticated methods for modelling the interactions between acoustic fields and bubbles [26,27], there still remain unknowns regarding the thermodynamic conditions needed for the onset of cavitation in HIFU. Similarly, the specific contributions of both temperature and pressure to this process and their own interactions are unexplored. Such gaps in the understanding of HIFU-induced nucleation hinders the ability to control and predict the spatial extent of the mechanical effects of HIFU bubbles, as much as estimating the timescales at which bubble-mediated phenomena take place.

One possibility for investigating bubble formation in HIFU fields is to use classical nucleation theory. The classical theory has been put aside in the field of biomedical ultrasound due to overestimated predictions for pressure thresholds under poor physical assumptions. Nevertheless, it has been recently shown that ultrasound cavitation can be modelled with the aid of CNT provided that the surface tension of water is corrected to an

effective value [15,28,29]. A similar approach has been successfully applied to therapeutic ultrasound [15]. This resulted in the development of what is referred to as the intrinsic threshold for cavitation in HIFU [29].

HIFU pressure and temperature fields are a unique scenario to study bubble nucleation. The possibility of subjecting small focal volumes to very negative pressures during short time intervals reduces the probability that minute impurities will affect the nucleation threshold [30]. The latter would be a case of heterogeneous nucleation (HEN). In HEN, impurities locally change the surface tension of the liquid and nucleation pressure thresholds often differ to those predicted by theoretical approaches. It is important to point out that, contrary to common belief, heterogeneous nucleation is not a phenomenon that necessarily reduces nucleation pressure thresholds. It has been argued in the literature that impurities can be of the destabilising type, which reduces nucleation pressure thresholds, or of the stabilising type, which increases these thresholds [28,31,32].

In this work, classical nucleation theory is employed to investigate the connection between the ultrasound protocol with the energetic requirements of bubble nucleation in HIFU and the thermodynamic properties of newly nucleated bubbles. As a case study, boiling histotripsy in tissue-mimicking phantoms is modelled [33]. Nonetheless, this methodology can be extended to the study of HIFU-induced bubble nucleation in most systems with high water content given appropriate parametrisation. Such a fundamental approach was chosen due to the unsuitability of macro-scale fluid dynamics to explain bubble formation, leaving reasonably complicated experiments as the only source of insight into HIFU-induced bubble nucleation [15,28,29]. Likewise, understanding the thermodynamics of bubble nucleation in HIFU pressure and temperature fields is arguably a key component in the planning of HIFU protocols in terms of defining safety windows and establishing best practices.

This paper addresses key components in the implementation of CNT for HIFU applications such as (a) the derivation of nucleation pressure thresholds from thermodynamic principles; (b) the approximations for the surface tension of the liquid; (c) the effects of ultrasound frequency and focal volume on the onset of nucleation and (d) the different physical mechanisms underlying bubble nucleation at high or low temperatures, i.e. boiling or cavitation respectively. Furthermore, HIFU pressure fields obtained from a Khokhlov–Zabolotskaya–Kuznetsov (KZK) model and temperature fields obtained via the Pennes' Bio-Heat Transfer Equation are plugged into CNT models. This allows the estimation of the timescales of bubble nucleation in boiling

histotripsy, spatial maps for nucleation pressure thresholds, the size of critical bubble nuclei at the HIFU focus and the prediction of the region where bubbles first nucleate.

2. Theory and Methods

2.1. The Critical Work of Nucleation

Liquids are notable for their ability to withstand tensile (negative) pressures before a gas phase appears, entering a metastable state [34]. Metastable liquid phases are those where the fluid is stretched beyond its vapour pressure or superheated above the boiling point [35,36]. In HIFU, both these mechanisms can induce liquid-phase metastability at the focus. Metastability is only viable because phase transformations are delayed by the energetic cost of creating an interface for a bubble in the bulk of a liquid [36]. This delay is manifested as an energy barrier which needs to be overcome before phase transitions take place [37].

The work required for the nucleation of a bubble of radius r in a liquid is given by [36]

$$W(r) = (4\pi r^2)\sigma + \left(\frac{4\pi r^3}{3}\right)(P_L - P') + \left(\frac{4\pi r^3}{3}\right)\frac{P'}{k_B T}\Delta\mu, \quad (1)$$

where σ is the liquid's surface tension, P_L is the pressure in the liquid, P' is the pressure inside a newly formed vapour nucleus, k_B is Boltzmann's constant, and T is the temperature in the liquid. The supersaturation of the system $\Delta\mu = \mu_L - \mu_V$ is represented by the difference in chemical potentials between the liquid and vapour phase. This equation is obtained under the assumption that vapours behave as ideal gases and the surrounding liquid is incompressible.

The size-dependent work needed to nucleate a bubble increases to a maximum at the critical radius of nuclei r^*, and then starts to decrease. This is represented mathematically as $dW/dr|_{r=r^*} = 0$. At this maximum, the bubble nucleus can be assumed to be in thermodynamic equilibrium with the liquid ($\Delta\mu = 0$) [38]. The critical size can be obtained by applying these conditions to Eq. 1, resulting in a Young-Laplace-type equation:

$$r^* = \frac{2\sigma}{P' - P_L}. \tag{2}$$

The critical work of nucleation W^* can then be derived by replacing r^* in Eq. 1 and considering thermodynamic equilibrium ($\Delta\mu = 0$):

$$W^* = \frac{16\pi}{3}\frac{\sigma^3}{(P' - P_L)^2}. \tag{3}$$

2.2. Nucleation Rates

The critical work for nucleation is used to predict the nucleation rate. This is the net rate at which bubbles reach the critical size and is proportional to the difference between the forward rates of vaporisation and the backward rates of condensation [39]. At sufficiently high nucleation rates, the control volume under consideration cannot be considered a single-phase volume anymore. The pressure and temperature in the liquid at this point can be seen as the nucleation threshold of this system.

Assuming that the timescales of nucleation are much shorter than the tensile period of the ultrasound wave, the nucleation rate can be approximated as a stationary quantity. This is an equilibrium average in time and space for the number of critical nuclei formed in the system under consideration. At the critical size, the steady-state nucleation rate is usually represented as [31]

$$J_S = J_0 \exp(-W^*/k_B T). \tag{4}$$

In this equation, the pre-exponential term J_0 accounts for the average kinetic and spatial properties of nucleation. It also defines, mathematically, an upper bound for the nucleation rate since $J_S \to J_0$ for $W^* \to 0$. On the other hand, the exponent is a thermodynamic term, describing the non-dimensional energy of formation of a critical nucleus. By neglecting the effects of viscosity and inertia in the liquid, J_0 can be defined in the form [36,39]

$$J_0 = N_0 \sqrt{\frac{2\sigma}{\pi m}}, \tag{5}$$

having $N_0 = \rho_L/m$ where ρ_L is the liquid density and m is the molecular mass of the liquid.

For steady-state nucleation, the number of critical nuclei Σ formed in the volume V_0 during a time interval τ_S can be approximated by

$$\Sigma = V_0 \int_0^{\tau_S} J_S(P_L, T)dt, \tag{6}$$

where J_S is the nucleation rate in a liquid at a pressure P_L and temperature T [36,40]. The definition of J_S in Eq. 4 is time independent, but the acoustic field causes P_L and T to be transient. Thus, we assume that the integration interval τ_s is sufficiently small so that no appreciable changes in J_S occur due to variations in T and P_L. Σ can then be approximated as

$$\Sigma \cong J_S V_0 \tau_S. \tag{7}$$

Considering the formation of the first Σ nuclei, we can define

$$J_S = \frac{\Sigma}{V_0 \tau_S}, \tag{8}$$

where J_S is the phenomenological nucleation rate for the appearance of Σ nuclei in a volume V_0 after τ_S seconds. Having that V_0 is a control volume where Σ bubbles nucleate after τ_S seconds, the value of this parameter is assumed to be the volume within the 3 dB drop in intensity at the transducer focus. Therefore, the choice of V_0 depends on the transducer geometry.

The quantity τ_S defines the time interval over which the first Σ bubbles nucleate. This is also referred to as the "mean-lifetime of the metastable fluid" [41,42], the "average time of formation of the first supercritical nucleus" [43] or the "experiment/observation time" at the steady state [44]. The attainable length of this quantity is known to decrease as metastability increases, making the measurement of thermodynamic properties deep in the metastable region difficult or even practically impossible [28,36].

Thermodynamically, the value of τ_S should be larger than the time-lag of nucleation, i.e. a measure of the timescales needed for the nucleation rate to reach its steady-state value given by Eq. 4. Values for the time-lag

158 of nucleation have been shown to be of the order of nanoseconds for vapour bubble nucleation in water [31].
159 Moreover, the choice of τ_S needs to be such that variations in P_L and T are minimal and these quantities can be
160 assumed nearly constant. Thus, parametrisation of τ_S is constrained by the interactions between the ultrasound
161 source, the propagating medium and resulting heat deposition.

162 Approximating the integral in Eq. 6 in the form of Eq. 7 means that, in HIFU, τ_S should be modelled as a
163 fraction of the ultrasound wave where pressure values are the lowest and remain reasonably constant. Therefore,
164 τ_S was approximated as $(1/10f)$, where f is the ultrasound frequency. This ensures that P_L variations within
165 this time interval are negligible, i.e. $P_L(t - \tau_S/2) \approx P_L(t) \approx P_L(t + \tau_s/2)$, where t is time. It also guarantees
166 that τ_S is sufficiently smaller than the timescales for gas diffusion in liquids, so diffusion can be neglected and
167 the nucleating medium is modelled as water.

168 The attenuation of sound waves in non-ideal, inhomogeneous media is given by the combined effects of
169 absorption, diffraction and scattering, following a power law with respect to the frequency [66]. Assuming $\tau_S =$
170 $(1/10f)$ will result in large values of τ_S at low frequencies (100 – 1000 kHz), which would allow sufficient
171 time for heat deposition in the medium and cause an increase in temperature. However, following the power
172 law of attenuation, absorption can be neglected at low frequencies and the focal region is thought not to undergo
173 significant temperature variations during τ_S. Conversely, acoustic absorption is appreciable in the megahertz
174 frequency range (1 – 10 MHz). Nonetheless, heat deposition can be equally neglected because τ_S is of the order
175 of nanoseconds and the focal temperature can be assumed nearly constant over such timescales.

176 2.3. Nucleation Pressure Thresholds

177 Having the nucleation rate J_S that forms the first Σ nuclei in a time-volume setup $V_0\tau_S$, a phenomenological
178 approximation to the nucleation pressure threshold of a liquid can be obtained by solving Eqs. 4 and 8 in terms
179 of the pressure in the liquid P_L. This approach for obtaining the temperature-dependent nucleation pressure
180 threshold $P_L^N(T)$ was first employed in [45] and has also been used in more recent publications [44,46].

181 The nucleation pressure threshold has also been referred to as tensile strength, cavitation pressure or intrinsic
182 threshold in the literature [24,29,38,42,45]. In this paper, the terminology "cavitation pressure/threshold" is
183 avoided. This is because such nomenclature has been mostly used to describe the phenomenon of detectable

bubble activity in a liquid that is not necessarily depleted of microbubbles [24]. Nucleation, on the other hand, is viewed as the mechanism by which a first-order phase transition happens [31].

Equating the thermodynamic (Eq. 4) and the phenomenological (Eq. 8) expressions for the nucleation rate, replacing the critical work of nucleation given by Eq. 3 and solving for P_L gives

$$P' - P_L^N = \left(\frac{16\pi\sigma^3}{3k_B T \ln\left(\frac{J_0 V_0 \tau_S}{\Sigma}\right)} \right)^{\frac{1}{2}}. \tag{9}$$

In this expression, P_L^N is the pressure P_L in the liquid at which an average of Σ nuclei appear during a time interval τ_S in a homogeneous volume of liquid V_0 at a temperature T. A Poynting correction allows the vapour pressure P_V of the liquid to be used instead of the nucleus internal pressure P' [38,39]. At high pressures, these are different quantities because of the assumption of thermodynamic equilibrium $\Delta\mu = 0$ used to obtain Eq. 3. The pressure drop $(P' - P_L)$ can be accurately approximated by

$$(P' - P_L) = \zeta(P_V - P_L) \tag{10}$$

having

$$\zeta = 1 - \left(\frac{\rho_V}{\rho_L}\right) + \frac{1}{2}\left(\frac{\rho_V}{\rho_L}\right)^2, \tag{11}$$

where ρ_V and ρ_L denote the saturated densities of vapour and liquid water, respectively [39].

The nucleation pressure threshold then assumes the form

$$P_L^N = P_V - \frac{1}{\zeta}\left(\frac{16\pi\sigma^3}{3k_B T \ln\left(\frac{J_0 V_0 \tau_S}{\Sigma}\right)} \right)^{\frac{1}{2}}. \tag{12}$$

This quantity can be evaluated by using standard thermodynamic quantities such as the vapour pressure of the liquid P_V and its density in the liquid and vapour phases. In order to calculate P_V, the International Association for the Properties of Water and Steam (IAPWS) expression for the vapour pressure of water was used [47]

$$\ln\left(\frac{P_V}{P_c}\right) = (\alpha_1 x + \alpha_2 x^{1.5} + \alpha_3 x^3 + \alpha_4 x^{3.5} + \alpha_5 x^4 + \alpha_6 x^{7.5}) T_r^{-1}. \quad (13)$$

199 In this equation, P_c is the critical pressure of water and $x = 1 - T_r$, where T_r is the reduced temperature T/T_c
200 having T_c as the critical temperature of water. The values for α are $\alpha_1 = 7.85951783$, $\alpha_2 = 1.84408259$, $\alpha_3 =$
201 11.7866497, $\alpha_4 = 22.680\,741\,1$, $\alpha_5 = 15.9618719$ and $\alpha_6 = 1.80122502$. For the calculation of P', the IAPWS
202 equations for the densities of the saturated liquid ρ_L and vapour phases of water ρ_V were employed such that

$$\rho_L = \rho_c(1 + b_1 x^{\frac{1}{3}} + b_2 x^{\frac{2}{3}} + b_3 x^{\frac{5}{3}} + b_4 x^{\frac{16}{3}} + b_5 x^{\frac{43}{3}} + b_6 x^{\frac{110}{3}}), \quad (14)$$

203 and

$$\ln\left(\frac{\rho_V}{\rho_c}\right) = c_1 x^{\frac{2}{6}} + c_2 x^{\frac{4}{6}} + c_3 x^{\frac{8}{6}} + c_4 x^{\frac{18}{6}} + c_5 x^{\frac{37}{6}} + c_6 x^{\frac{71}{6}}. \quad (15)$$

204 In Eqs. 14 and 15, ρ_c is the critical density of water. The values for constants b given by $b_1 = 1.99274064$,
205 $b_2 = 1.09965342$, $b_3 = -0.510839303$, $b_4 = -1.75493479$, $b_5 = -45.5170352$, $b_6 = -6.74694450\times10^5$. The
206 values of c are as follows $c_1 = -2.03150240$, $c_2 = -2.68302940$, $c_3 = -5.38626492$, $c_4 = -17.2991605$, $c_5 =$
207 -44.7586581, and $c_6 = -63.9201063$.

208 ## 2.4. The Effective Surface Tension

209 Equations 3, 4 and 12 show, respectively, the dependence of the nucleation work, nucleation rate and the
210 nucleation threshold on the liquid's surface tension σ. Indeed, the surface energy is a substantial component of
211 the energetics of nucleation. Under special assumptions, it can be shown that W^* equals about one third of the
212 surface energy of the metastable liquid in question [31]. The surface tension is a macroscopic manifestation of
213 the cohesion of matter [48]. The high surface tension of water, for instance, is thought to be connected to strong
214 hydrogen bonds and the high energies involved in breaking and rearranging them into a surface [49].

215 The actual surface tension σ of bubbles at the moment of nucleation is thought to be size, pressure and
216 temperature dependent [31,50,51]. However, it is common to approximate it with a temperature-dependent

planar surface tension $\sigma_\infty(T)$ in CNT. An expression for σ_∞ can be obtained from a revision of the 1994 IAPWS Secretariat release [52]

$$\sigma_\infty(T) = \sigma_1(1 - T_r)^{\sigma_2}\,[1 + \sigma_3(1 - T_r)], \tag{16}$$

In Eq. 16, σ_1 = 235.8 × 10^{-3} Nm^{-1}, σ_2 =1.256 and σ_3 = -0.625.

In CNT, expressions for the surface tension like Eq. 16 are traditionally used for modelling boiling and cavitation [28,38]. The planar surface tension σ_∞ is the limiting value of σ for $r \to \infty$, i.e. a planar interface. This is referred to as the capillarity approximation [31,53]. It is important to highlight that the capillarity approximation is heuristic and not intrinsic to CNT [36,53,54].

Indeed, the discrepancy between theoretical and experimental results in the nucleation of bubbles in water has been consistently associated with the capillarity approximation [31,48-51,55]. If the capillarity approximation is used, CNT predicts tensile pressures of about -150 MPa for bubble nucleation in water at ambient temperature, whereas most experiments do not surpass -40 MPa [34]. Furthermore, CNT models are unable to account for a vanishing energy barrier $-W^*/k_BT$ as the liquid approaches its limit of stability, called the liquid spinodal [56,57]. Alternative approaches have been developed to account for this shortcoming in CNT's implementation. Density-functional theory (DFT) [50,51] models the continuous change in density between the liquid and vapour phases, and does not evoke a capillarity approximation. Alternatively, molecular dynamics (MD) simulations [41,42,49,54] model nucleation from the attractive-repulsive forces between molecules.

Researchers have also attempted to find phenomenological scaling factors which could correct the surface tension or the nucleation work so these would match experiments [38,57]. Recently, nucleation rates obtained in sophisticated HIFU experiments have been used in Eq. 4 in order to approximate an "effective value" of σ_∞ up to temperatures of 200 ˚C [28]. These experiments found that using a surface tension approximated by 23.7% of σ_∞ could model HIFU nucleation pressure thresholds in CNT with a good agreement to experimental results. Similar experiments have been performed more recently up to 90˚C [29]. The latter reported similar results, however with a scaling value ranging from 25% to 27.5% for the surface tension of water.

Drawing from these findings, a temperature-dependent scaling factor c_E for the surface tension was calculated such that $\sigma_E = c_E(T)\sigma_\infty(T)$. This methodology was found to harmonise CNT and HIFU experimental results with better accuracy than a single scaling value for all temperatures. This was achieved by optimising in c_E the absolute error between analytic predictions of Eq. 12 and experimental data for nucleation pressure thresholds in acoustic fields from aforementioned studies.

Using temperature-dependent HIFU nucleation pressure thresholds from experimental works in the literature [28-30,58], $c_E(T)$ was calculated by minimising the absolute error given by Eq. 17 for each temperature.

$$E\big(c_E(T_{EXP})\big) = \sqrt{(P_L^N(T_{EXP}, c_E) - P_{EXP})^2}. \quad (17)$$

In Eq. 17, P_{EXP} and T_{EXP} represent, respectively, experimental values of the nucleation pressure threshold and the temperature at which they were obtained. Moreover, $P_L^N(T_{EXP}, c_E)$ represents the predictions of Eq. 12 for pressure thresholds at a temperature T_{EXP} and a scaling factor c_E. In this work V_0 was calculated as an ellipsoidal focal volume within the - 3dB drop region for a 2 MHz HIFU transducer (Sonic Concepts H106) as specified by the manufacturer.

Values of c_E previously published in the literature use either a constant kinetic term [59] or have been obtained as a single value for a wide temperature range [28]. Herein, data from the aforementioned studies is combined with a pressure and temperature-dependent kinetic factor in order to obtain a linear dependence for c_E on the liquid's temperature. For $0\ °C < T < 90\ °C$, this relationship reads:

$$c_E(T) = 0.4869 - 6.1425 \cdot 10^{-4}(T + 273.15), \quad (18)$$

where T is the temperature in Celsius.

It follows that the effective surface tension for HIFU-induced bubble nucleation is approximated as $\sigma_E(T) = c_E(T)\sigma_\infty(T)$. For temperature values between 90 and 110 °C, c_E is extrapolated based on Eq. 18. For temperature values above 110 °C a conservative approach is taken and a constant c_E is assumed, such that $c_E(T > 110\ °C) = c_E(110\ °C)$.

3. Results and Discussion

3.1. The Effects of the Surface Tension on Nucleation Pressure Thresholds

Figure 1-A compares P_L^N values obtained for $c_E\sigma_\infty$ (solid line), values obtained for a scaled planar surface tension as 24% and 28% of σ_∞ [28,29] and experimental results in HIFU nucleation [28-30,58]. Fig. 1-A shows the better agreement of P_L^N to experimental results for the temperature-dependent c_E given by Eq. 18. Values of P_L^N obtained for scaling at 24% and 28% of σ_∞ are good approximations for the order of magnitude of P_L^N however fail to be consistent throughout the temperature range of interest in HIFU applications.

Moreover, Fig. 1-B compares the values of P_L^N obtained from a planar surface tension (dashed and dotted line) with a temperature-dependent "effective" surface tension $c_E\sigma_\infty$ (solid line). White circles represent the liquid spinodal pressure of water obtained from DFT simulations for the five-site transferable interaction potential (TIP5P) equation of state [55]. This is an equation of state derived from the TIP5P model of water, describing its properties within the realm of molecular dynamics at low temperatures. It can be seen in Fig. 1-B that nucleation pressure thresholds calculated using σ_∞ yield quantities far below the spinodal pressure of liquid water [34,60,61].

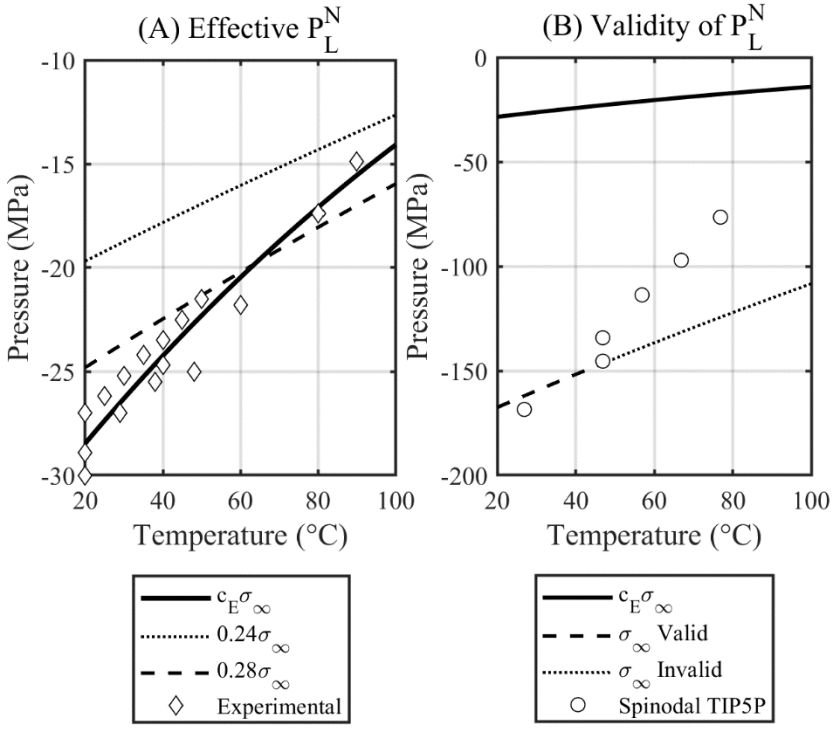

Figure 1. (A) Comparison between a temperature-dependent scaling $c_E(T)$ given by Eq. 18 for the surface tension to constant values of 24% and 28%. (B) Temperature-dependent nucleation pressure threshold in water for a planar surface tension σ_∞ given by Eq. 16 and an effective surface tension $c_E\sigma_\infty$ obtained with Eqs. 16 and 18. Dotted values show CNT predictions which are below the liquid spinodal pressure of water obtained by the TIP5P, which is represented in white circles.

This a known limitation of CNT if the surface tension is approximated with size-independent expressions, such as the planar surface tension approximation. In these cases, CNT is not able to account for a vanishing work of nucleation W^* as pressures approach the spinodal pressures of water [31]. The spinodal of a liquid is the limit between its metastable and unstable regions. As the liquid's pressure approaches the spinodal, density fluctuations grow without limit due to a divergent liquid compressibility [44]. It follows that at the spinodal, the free energy barrier that delays nucleation disappears, and a new phase forms spontaneously in an alternative process to nucleation, termed spinodal decomposition [36]. Therefore, predictions of P_L^N that are below the values for the spinodal pressure of water should be deemed invalid.

3.2. Physical Rationale for Nucleation Pressure Thresholds and the Regimes of Boiling and Cavitation

In Fig. 2, the steady-state nucleation rate given by Eq. 4 is shown as a function of temperature for several pressure contours (-40, -30, -20, -10 and -5 MPa) in 2-A, and as a function of pressure for several temperature contours (25, 50, 100, 150 and 250 °C) in 2-B. These values are in units of the number of bubble nuclei per millimetre cubic per 0.1 microseconds, which are length and timescales compatible with HIFU.

The dashed line indicates the formation of at least one bubble nucleus ($\Sigma = 1$) in an ellipsoidal volume V_0 =1.73 mm^3 after a time interval of $\tau_S = (1/10f)$ =50 ns for a given pressure-temperature pair. This approximation for V_0 is valid under the assumption that the focus of a 2 MHz transducer (Sonic Concepts, H106) is an axisymmetric ellipsoid with axial and lateral half width dimensions of 2.86 and 0.365 mm, as specified by the manufacturer.

Figure 2 exemplifies the phenomenological approach to nucleation used in this work. Eq. 4 states that any given pair of pressure and temperature (P_L, T) will be associated to a certain nucleation rate $J_S(P_L, T)$. Moreover, Eq.

8 postulates that there is a critical value of J_S which is approximately $\Sigma/V_0\tau_S$ at which the system cannot be considered single-phased anymore.

For $\Sigma = 1$, this value is marked by a dashed line in Fig. 2. Thus, at a given temperature T, a nucleation pressure threshold P_L^N is the value of the pressure in the liquid for which the curve of J_S given by Eq. 4 intersects the line given by $1/V_0\tau_S$. Values of J_S above $1/V_0\tau_S$ indicate nucleation rates which can be interpreted as bubble formation, whilst values below it indicate rates that are too low for the onset of bubble activity. It is important to highlight that within the current phenomenological implementation where J_S is obtained for a pure liquid, values of $J_S \gg 1/V_0\tau_S$ are more theoretical than of practical value.

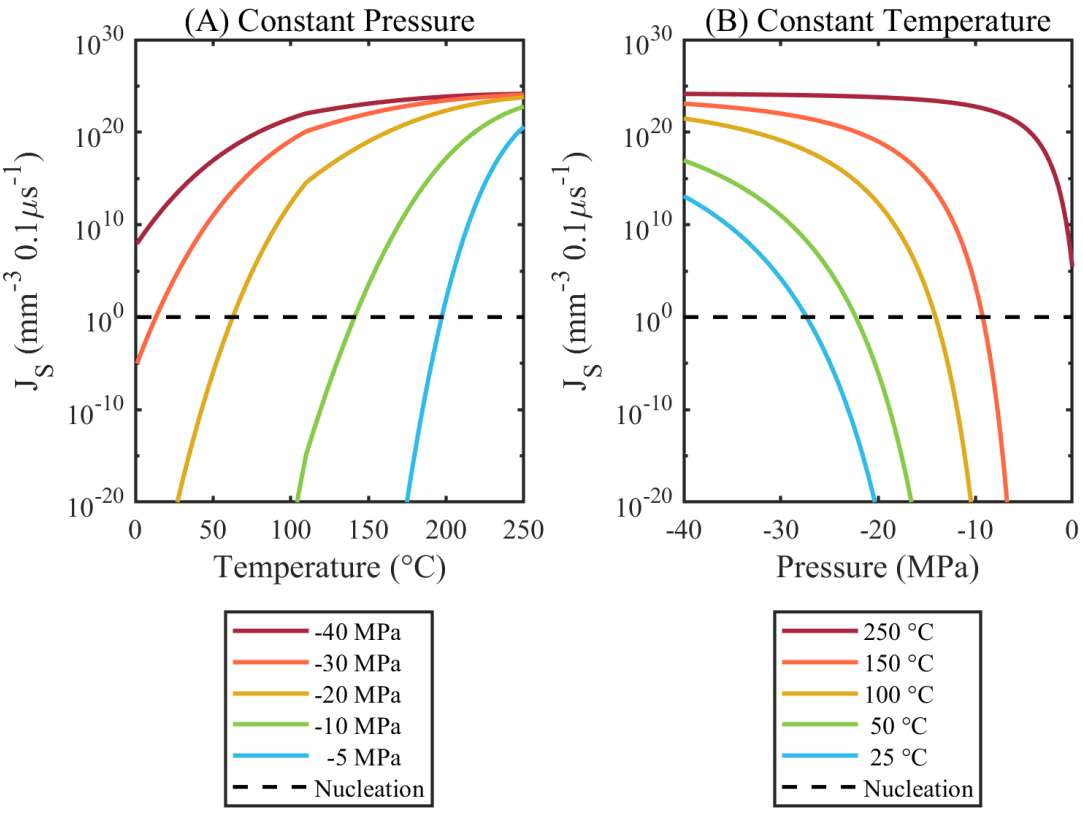

Figure 2. Effects of pressure and temperature on the nucleation rate.

Results in Fig. 2 show how pressure and temperature affect the nucleation rate in different ways depending on the thermodynamic state of the liquid. Fig. 2-A shows that at temperatures above 100 °C, a 10 MPa change in pressure will not have as significant of an effect in J_S than it would at temperatures lower than 50 °C, as shown

by the contours of -40, -30 and -20 MPa. In such a case, nucleation at high temperatures is controlled by the superheating of the system.

This can be further verified by noticing that the curves for -40 and -30 MPa plateau at temperatures much lower than those for -20, -10 and 0 MPa in Fig. 2-A. Indeed, the curves of the nucleation rate as a function of temperature are steeper at less negative pressures (-20, -10 and -5 MPa). This indicates behaviour similar to explosive boiling: appreciable increases in the nucleation rate for small temperature variations. These are important trends that should be kept in mind, considering that in the presence of non-linear heating some HIFU protocols are notable for inducing temperature rises of over 60 °C in a few milliseconds [11].

Moreover, it can be seen in Fig. 2-B that for nucleation at very negative pressures, a change in temperature will not affect J_S significantly at high temperatures (100-250 °C). In contrast, nucleation rates are at least 5 orders of magnitude higher between temperature contours of 50 and 25 °C. This indicates that the pressure of the liquid becomes more relevant in nucleation at lower temperatures. A similar trend was also observed in a sonocrystallisation process where solid crystals are created out of a supersaturated solution exposed to ultrasound [72,73]. The authors reported that the effect of pressure on nucleation is more pronounced at lower supersaturation ratios.

These results explain how HIFU-induced bubble nucleation can be driven by two factors: very low pressures [15] or high temperatures [11]. Indeed, histotripsy protocols have been broadly named cavitation-cloud histotripsy (CCH) and boiling histotripsy (BH), deriving from the sense that bubble nucleation at high temperatures is termed boiling and bubble nucleation at lower temperatures and very low pressures is termed cavitation. Results shown in Fig. 2 corroborate with this terminology, showing that stretching and heating the system affect the nucleation rate in different ways depending on the initial temperature of the system.

3.3. Effects of Ultrasound Frequency on Pressure Thresholds

The interpolation for c_E in Eq. 18 was obtained for HIFU nucleation data performed at frequencies lower than 2 MHz. It is therefore important to assess the effects of the ultrasound frequency in nucleation when using CNT. In this study, the mean lifetime of the metastable fluid τ_S is, effectively, the time the fluid is placed at nearly constant pressure and temperature before nucleation. The dependence of the nucleation pressure threshold P_L^N

on the mean-lifetime of a metastable fluid described by Eq. 12 is shown in Fig. 3 as a function of frequency, where $\tau_s = (10f)^{-1}$. From Eq. 12, the magnitude of P_L^N is expected to decrease at slow rates for an increasing mean lifetime τ_S [45]. This dependence describes the time interval needed for underlying energetic phenomena to take place in nucleation, and is not related to bubble oscillations in an acoustic field. Such a trend somehow agrees with the predictions of the Mechanical Index (MI) [16]. The MI states, following from experimental observations, that ultrasound-induced cavitation is more likely at lower frequencies.

Figure 3 shows P_L^N at 38 °C as a function of the ultrasound frequency from 0.1 Hz to 10 MHz and the focal volume from 1 mm^3 to 1 cm^3. The vector gradient in Fig. 3-A shows a greater decrease in the magnitude of P_L^N in the direction of bigger volumes and lower frequencies. This means that the nucleation pressure threshold decreases at lower frequencies. As an example, the difference in P_L^N at 20 °C between 1 MHz and 2 MHz is approximately 0.16 MPa for a focal volume of 1 mm^3 and approximately 0.14 MPa for a focal volume of 1 cm^3. The effects of frequency and focal volume are reduced at higher temperatures. At 100 °C, these difference, drop, respectively, to 0.082 and 0.069 MPa.

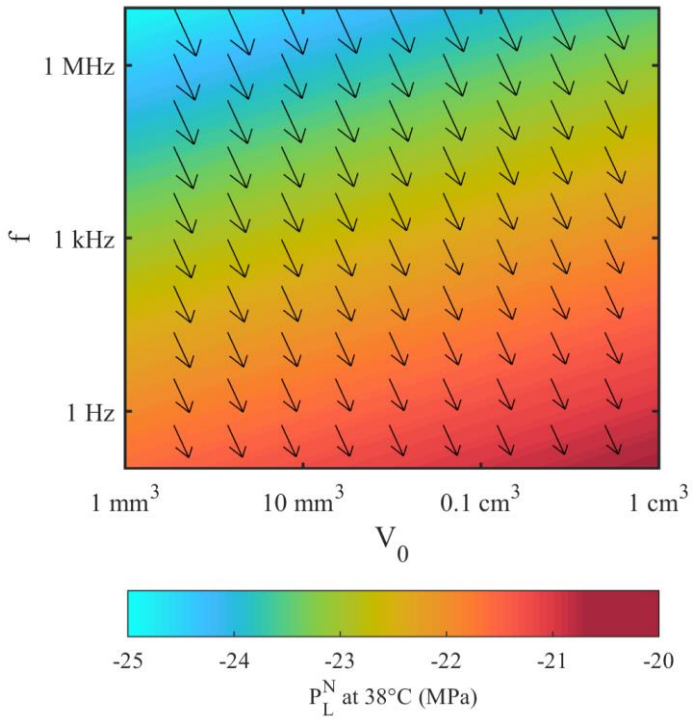

Figure 3. Effects of frequency and focal volume on nucleation thresholds at 38 °C.

In summary, the results presented above show that although the ultrasound frequency does play a role in determining the energetics of nucleation, this is of secondary importance to the temperature of the medium. It was also shown that nucleation pressure thresholds are decreased at lower frequencies for a fixed focal volume and constant temperature. This is in agreement with previous experimental work on the effects of frequency on bubble nucleation [62]. Finally, the results shown in Fig. 3 confirm that although $c_E(T)$ was calculated for experimental results performed at lower frequencies, c_E is still valid for modelling HIFU nucleation at 2 MHz.

3.4. Acoustic Propagation and Heat Deposition in Tissue-mimicking Phantoms

The HIFU Simulator 1.2 [63] was employed to solve a Khokhlov–Zabolotskaya–Kuznetsov (KZK) nonlinear acoustic wave equation and obtain pressure waveforms and the absorbed ultrasound energy for a HIFU pressure field. The KZK equation is often used to model high-intensity acoustic beams and has been successfully applied for modelling acoustic fields for HIFU and lithotripsy sources [64-66]. This equation approximates nonlinearity and thermoviscous absorption within a plane wave approximation and also diffraction in a parabolic approximation [66]. From the absorbed acoustic energy obtained with the KZK equation, the temperature rise at the focus can be calculated with the Pennes Bio-Heat Transfer Equation (BHTE). This equation models heat deposition at the HIFU focus accounting for heat diffusion and convective cooling due to blood perfusion [66]. In the present work, the convective term in the BHTE is ignored due to the absence of perfusion, and this equation is reduced to a simple heat diffusion equation in the presence of a heat source.

Non-linear acoustic propagation and heat deposition in a tissue-mimicking gel were simulated for a single element focused transducer operating at 2 MHz (Sonic Concepts H106). Tissue-mimicking phantoms have been extensively used for experimental work on histotripsy, having found good agreement with ex-vivo results [10,65,67]. The transducer and medium parameters for the HIFU Simulator were taken from previous works on boiling histotripsy [10,33,65] and ultrasound-induced nucleation [28,30,44]. Propagation was simulated for a two-layer medium, first in water and then in phantom for an input electrical power of 150 W and 85% transducer efficiency. Following manufacturer specifications for a 2 MHz transducer (Sonic Concepts, H106), the radius of curvature was 63.2 mm, where the final 5 mm accounts for propagation through the phantom. The linear pressure gain for the focused transducer was 72.9 [65].

The spatial grid consisted of 20 points per wavelength in the axial direction and 25 points per wavelength in the radial direction for a total domain length of 9.48 cm. The upper half of the axisymmetric domain consisted of 438 elements in the radial direction and 2062 elements in the axial direction, resulting in 903,156 elements. Element sizes were of 0.0731 and 0.0460 mm in the radial and axial directions, respectively. Simulations were carried for 128, 256, 512, 1024 and 2048 harmonics. Results were considered to converge when doubling the number of harmonics yielded less than 0.5% difference in peak positive pressure (PPP) amplitudes. Pressure fields obtained for 2048 harmonics were chosen to be incorporated into the CNT models discussed in this work.

HIFU heat deposition was calculated with BHTE equations, which in absence of a convective sink are reduced to standard heat diffusion equations with a heat source given by the absorption of pressure waves. Temperature fields were computed up to 20 ms of HIFU sonication for each element in the grid for an initial temperature of 20 °C. These temperature maps were then used to calculate the thermodynamic quantities given by Eqs. 2 – 5, Eqs. 10 – 16 and Eq. 18 at each element of the mesh.

3.5. The Timescales of Nucleation in HIFU

The timescales of boiling bubble nucleation in HIFU have been traditionally approximated by the pulse duration the focal region needs to reach 100 °C [2,3,33,65,68]. This approximation carries the underlying assumption that bubbles always nucleate at 100 °C independently of the pressure of the medium. Such an assumption does not have much physical reasoning other than the empirical observation that tap water boils at about 100 °C under atmospheric pressure. It is important to notice that liquids or tissue phantoms are traditionally degassed before HIFU experimentation, depleting the medium from microbubbles which trigger boiling at 100 °C under atmospheric pressure [24]. Appropriate parametrisation and planning of boiling histotripsy, therefore, need to account for the timescales necessary to cause explosive boiling within milliseconds in terms of focal pressures and temperatures [69].

Figure 4-A shows the nucleation pressure threshold calculated at the HIFU focus as a function of the peak focal temperature, which increases with time due to heat deposition and is shown in Fig. 4-B. It can be seen in Fig. 4-A that heat deposition causes the nucleation pressure threshold P_L^N at the HIFU focus to decrease with pulse duration. The onset of nucleation will happen whenever the value of P_L^N is lower in magnitude than the peak

negative pressure at the HIFU focus, which is -15.71 MPa for the protocol under consideration and is represented by the black dashed line in Fig. 4-A.

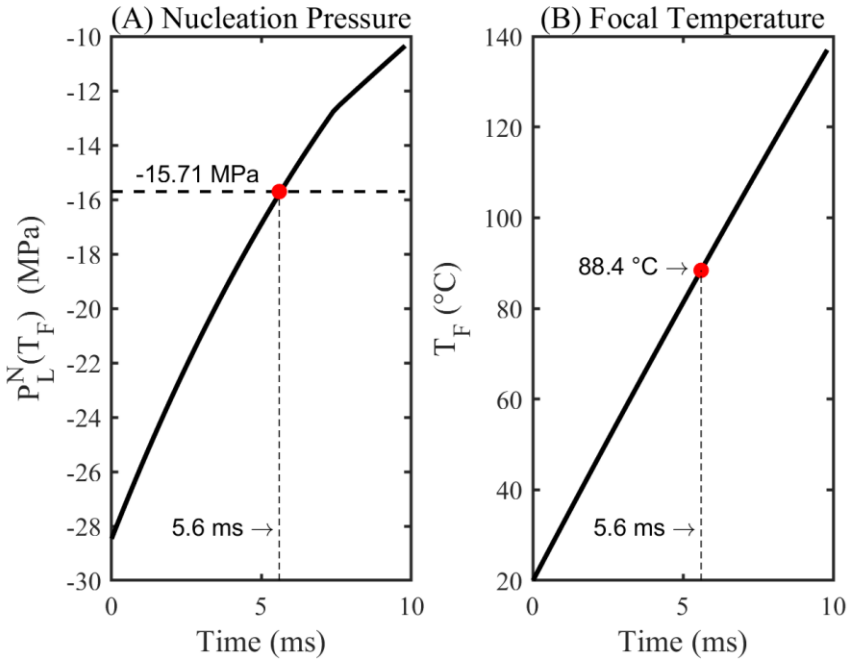

Figure 4. (A) Evolution in time of the nucleation pressure threshold at the HIFU focus at 66.72 kW cm^{-3} heating rates. (B) Evolution in time of HIFU peak temperatures.

Nucleation at 2 MHz driving frequency with P^+ = 83.54 MPa and P^- = -15.71 MPa is predicted after 5.6 ms of sonication in Figure 4. When these results are compared to those in Fig. 4-B, it can be seen that the simulated temperature of the medium at 5.6 ms of sonication is around 88.4 °C. This shows the possibility of nucleation in boiling histotripsy before the medium reaches 100 °C. These results indicate that boiling histotripsy, when performed within a few milliseconds, has similar origins to that of cavitation below the intrinsic threshold. However, BH would occur due to a lowering of the intrinsic threshold which is a consequence of heat deposition.

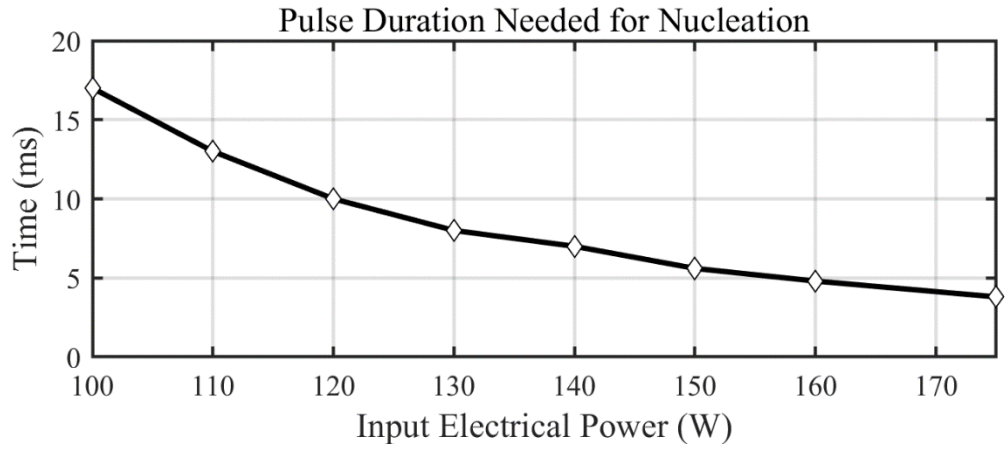

Figure 5. Pulse duration needed for the onset of nucleation as a function of input electrical power.

Additional simulations at 100, 110, 120, 130, 140, 160 and 175 W input electrical power were also performed for comparison with the results shown in Figure 4. A change in these parameters results in distinct HIFU pressure and temperature fields which shape the conditions under which nucleation happens. Figure 5 shows the pulse duration needed to trigger nucleation for a range of input electrical powers to the transducer.

Figure 5 shows that the pulse duration needed for nucleation decreases monotonically with increasing input electrical power to the transducer. In practice, such trends can inform the choice of appropriate PRFs and duty cycles in terms of the input electrical power when planning histotripsy protocols.

These results agree with the experimentally observed tendency of nucleation to take place at shorter timescales for high input electrical powers (large focal peak pressures) [10, 65]. Moreover, the trend in Fig. 5 is slightly non-linear because the focal waveforms become increasingly distorted for higher electrical power inputs to the transducer. This means that the magnitude of focal peak negative pressures does not increase as much as that of peak positive pressures for increasing input electrical power.

These results indicate that boiling histotripsy, when performed within a few milliseconds, has similar origins to that of cavitation below the intrinsic threshold. However, BH would occur due to a lowering of the intrinsic threshold which is a consequence of heat deposition. This means that within millisecond timescales it is difficult to draw a boundary between thermal and mechanical effects of HIFU in the nucleation of bubbles.

Consequently, the onset of nucleation at the HIFU focus depends both on the peak negative pressure of the ultrasound wave and on the temperature of the medium. This suggests that there is a high likelihood of not

obtaining millisecond bubble formation if peak negative pressures are below the nucleation pressure threshold. Finally, it is also worth noting that the limiting nucleation rates used to define pressure thresholds were of one bubble per millimetre cubic per 0.1 microseconds. As discussed above, these results will change if the observation timescales for nucleation τ_S are changed. However higher values of τ_S would require a transient expression for the nucleation rate and consideration of the effects of gas diffusion.

3.6. Spatial Profile of Nucleation

Following from models predicting nucleation after 5.6 ms, Fig. 6 shows the spatial profile of nucleation in terms of the acoustic pressure, the focal temperature and the temperature-dependent nucleation pressure threshold obtained around the geometrical focus. The KZK model showed this region to be that of highest heat deposition and lowest acoustic pressures. Figure 6-A shows the relationship between the preferential nucleation site (black dashed contours) to the peak negative acoustic pressures. The temperature-dependent nucleation pressure threshold is shown in Fig. 6-B, and the temperature distribution around the geometrical HIFU focus after 6 ms of sonication is shown in Fig. 6-C.

Figure 6-A shows that although the lowest acoustic pressures happened pre-focally (red dashed contour), the preferential nucleation site was placed around the HIFU focus at 6.36 cm in the propagation direction. This is somehow counter-intuitive to the idea that HIFU bubble nucleation is associated with the lowest acoustic pressures in the field.

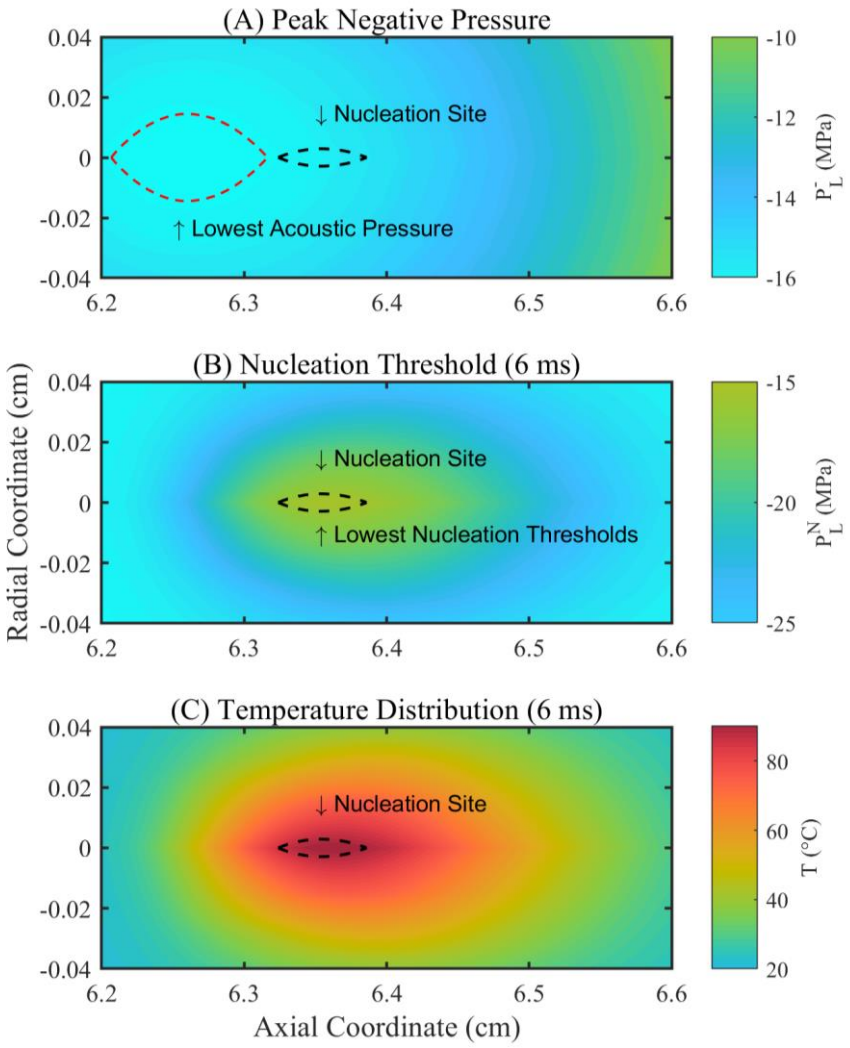

Figure 6. (A) Peak negative acoustic pressures obtained from KZK simulations. Black dashed contour demarks preferential nucleation sites. Red dashed contour demarks lowest acoustic peak negative pressures. (B) Nucleation pressure thresholds obtained from coupled KZK-BHTE-CNT simulations. Black dashed contour demarks preferential nucleation sites. (C) Temperature distribution after 6 ms of sonication obtained from KZK-BHTE simulations. Black dashed contour demarks preferential nucleation sites.

Figures 6-B and 6-C shed some light into this question. Figure 6-B shows that pre-focal nucleation thresholds after 6 ms of sonication vary from -25 to -20 MPa. The magnitude of these thresholds is much greater than the magnitude of the peak negative acoustic pressures that are shown in Fig. 6-A, which varies from -16 to -14 MPa in the same region. Therefore, nucleation as a consequence of acoustic propagation itself should not happen in these regions. Figure 6-B also shows that nucleation pressure thresholds have their lowest magnitude around the HIFU focus, where peak negative acoustic pressures surpass the threshold and trigger nucleation.

Finally, Fig. 6-C clarifies the disparity between nucleation preferential sites and lowest peak negative acoustic pressures shown in Fig. 6-A. Figure 6-C shows the temperature distribution after 6 ms of sonication. These results show higher temperatures at the geometrical HIFU focus, having the preferential nucleation site as an envelope to the regions of higher temperature. Since the nucleation pressure threshold is temperature-dependent, these results indicate that the regions of highest temperature are the regions where nucleation is more likely to occur within milliseconds given that acoustic pressures surpass the nucleation pressure threshold.

In summary, Fig. 6 shows that nucleation is spatially restricted to regions where the peak negative acoustic pressure overcomes the nucleation pressure threshold, however, these regions are not necessarily the regions of lowest acoustic pressure. Such results further indicate that bubble nucleation in boiling histotripsy is a phenomenon limited by temperature at the HIFU focus. This agrees with previous simulations of bubble dynamics in boiling histotripsy, which concluded that the temperature field can also limit the growth of BH bubbles [71]. Finally, it can be seen that although the acoustic pressure is the ultimate trigger for nucleation, HIFU heat deposition facilitates bubble nucleation. Thus, nucleation happens preferentially at the regions of highest heat deposition.

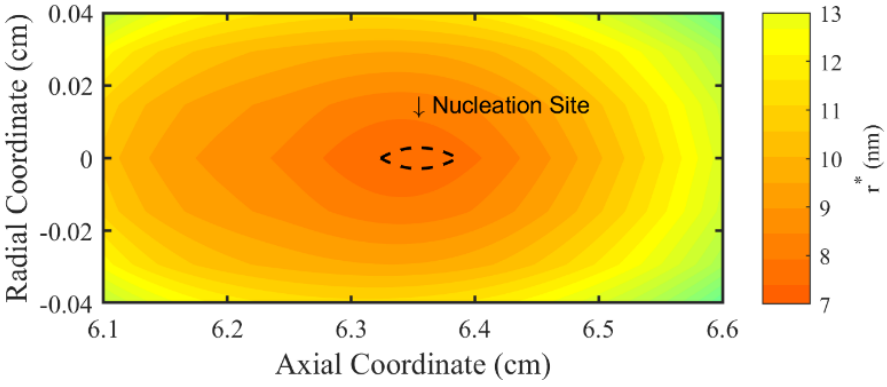

Figure 7. Size of critical nuclei around the HIFU focus.

Figure 7 shows the critical size of nuclei around the HIFU focus. This is the minimum size that nuclei must achieve such that their chances of spontaneous growth are greater than their chances of collapse. Within the preferential nucleation site, the radius of critical nuclei is of approximately 7.5 nm. These dimensions are in agreement with size stability bounds for bubble dynamics simulations of nano-bubbles in the literature [70]. Moreover, Fig. 7 also shows that bubbles nucleated at the HIFU focus following heat deposition tend to be

larger. This implies that the HIFU focus is the site where bubble nuclei have higher chances of merging with other nuclei of similar size and form larger bubbles which are mechanically stable within the thermodynamic conditions imposed by HIFU pressure and temperature fields.

It is important to note that the ability of Eq. 2 to predict the size of critical nuclei shown in Fig. 7 has limitations. This is an equation that predicts the minimum size of bubble nuclei so that nucleation happens. Equation 2 does not take into account either inertial or viscous terms present in standard equations for bubble dynamics [26,71]. This highlights the need to integrate these terms into CNT for realistic physical modelling of nucleating bubble dynamics.

3.7. The Effects of Pulse Duration on the Dimensions of the Nucleation Site

In Fig. 8, the effects of pulse duration on the length and width of the preferential nucleation site are displayed. Figure 8-A shows the length of the nucleation site which is zero at any time before the time of nucleation (5.6 ms) and then ranges from 0.62 mm after 6 ms of sonication to 2.69 mm after 20 ms of sonication. Similarly, Fig. 8-B shows the width of the preferential nucleation site. These range from 60 μm after 6 ms of sonication to 0.64 mm at 20 ms of sonication. These are not measures of the resulting cavity after a boiling histotripsy protocol, but rather an estimation of the region where boiling bubbles first originate and are thermodynamically stable within the HIFU-induced pressure and temperature fields.

In Fig. 8-C, the ellipsoidal volume of the nucleation site is computed based on its length and width. It can be seen that the total volume where bubbles first nucleate and are stable within the HIFU pressure and temperature field increases with pulse duration. This is equivalent to saying that the volume of the nucleation site increases with the size of the region where acoustic pressures surpass the nucleation threshold. As a consequence of the spatial profile of heat deposition in HIFU, the length of the nucleation site is consistently larger than its width. This can be observed in Fig. 8-D, showing that for very short protocols the length of the nucleation region is much larger than its width. For longer pulse durations, this ratio diminishes and the curve reaches what seems to be asymptotic behaviour at a ratio of approximately 4. These results flag a greater need for control and planning of boiling histotripsy lesions along the propagation direction rather than in the perpendicular plane (radial coordinate of the HIFU beam).

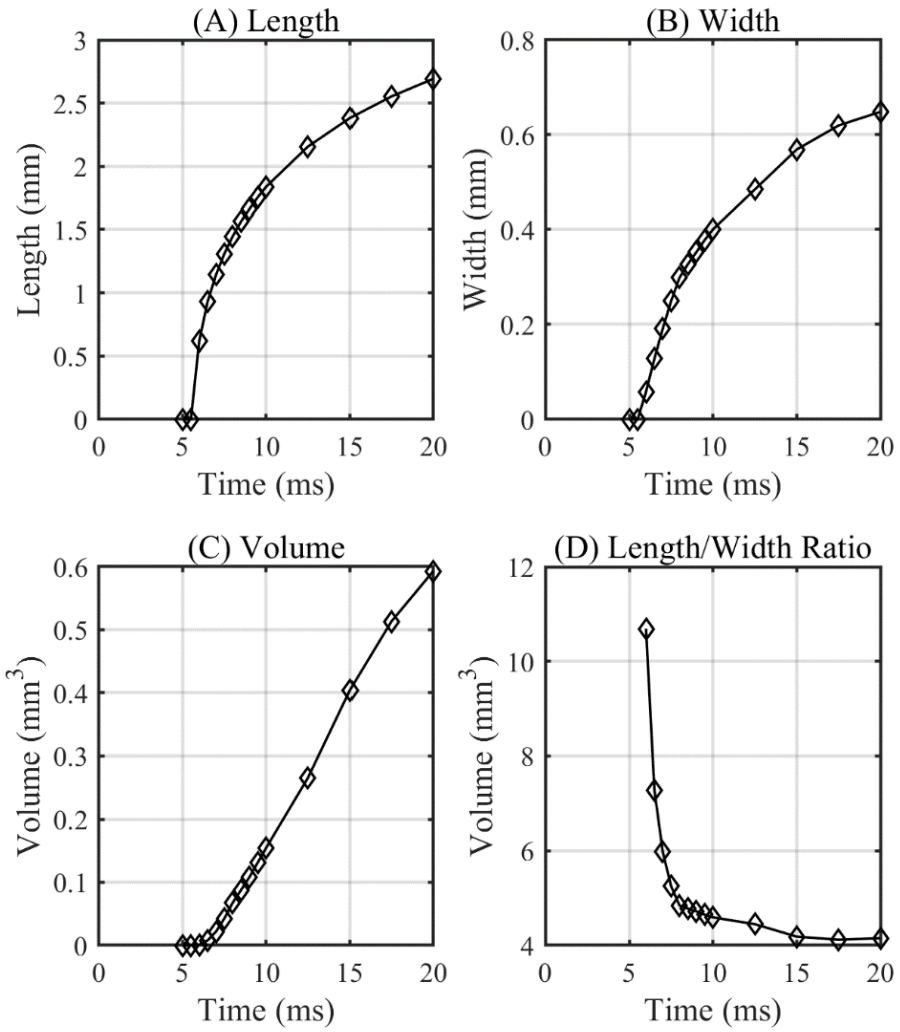

Figure 8. Dimensions of the nucleation site. (A) Length of the nucleation site. (B) The width of the nucleation site. (C) The volume of the nucleation site assuming ellipsoidal shape. (D) The ratio between the length and width of the nucleation site. Diamond markers in Fig. 8 represent values obtained for thermal simulations interpolated as the black solid line.

Results shown in Fig. 8 might also provide an explanation for the characteristic “tadpole” shape of boiling histotripsy lesions. Previous experiments on boiling histotripsy in tissue phantoms captured by high-speed cameras have shown that the tail of BH lesions is caused by the action of vapour bubbles [33]. Similarly, results in Fig. 8-D show that the length of the region where vapour bubbles nucleate is at least four times larger than the width where they can nucleate and grow spontaneously. The dimensions of this region would, therefore, influence the final shape of a BH lesion.

4. Conclusions

In this work, classical nucleation theory was applied to study bubble nucleation in HIFU pressure and temperature fields, using boiling histotripsy as a case study. A temperature-dependent expression for the nucleation pressure threshold in HIFU was derived from first principles assuming stationary nucleation. The importance of obtaining a suitable approximation for the surface tension of the liquid in obtaining nucleation pressure thresholds was discussed.

A temperature-dependent scaling factor for the surface tension in HIFU-induced nucleation was obtained by fitting available experimental data to the theoretical predictions of CNT. The effects of HIFU frequency and focal volume were analysed. It was found that the magnitude of nucleation pressure thresholds decreases with decreasing frequencies, however this effect is reduced at high temperatures.

It was shown that the regimes of boiling (nucleation triggered by high temperatures) and cavitation (nucleation triggered by negative pressures) can be distinguished in terms of the nucleation rate. At high temperatures ($T >$ 150 °C), the superheating of the system is the dominant factor in nucleation. Conversely, at medium and low temperatures ($T < 100$ °C) the peak negative acoustic pressure plays an increasingly important role in the nucleation of bubbles.

This means that when nucleation takes place at millisecond timescales and within the thermodynamic range of boiling histotripsy, the effects of HIFU-induced pressure and temperature fields are coupled and there is no clear dominance of either. Our models show that the acoustic pressure is the ultimate trigger for nucleation, however, HIFU heat deposition facilitates bubble nucleation by lowering thresholds. This is the reason why nucleation happens at the regions of highest heat deposition in BH. Moreover, it was also shown that bubble formation in boiling histotripsy can be achieved at temperatures lower than 100 °C provided that peak negative pressures surpass the nucleation threshold. These results indicate that the boundaries between boiling and cavitation-cloud histotripsy are much more diffuse than currently assumed.

The characteristic length and width of the preferential nucleation site were analyzed in terms of the pulse duration. These showed that the region where bubbles nucleate increases with pulse duration, depending ultimately on the temperature profile around the HIFU focus. The lengths of the preferential nucleation site in

terms of pulse duration were consistently greater than the width. This can provide an explanation for the formation of the tail of characteristic tadpole-shaped BH lesions.

5. Acknowledgements

MOdA would like to thank CNPq, the Brazilian National Council for Scientific and Technological Development for funding their PhD at UCL.

References

1. Maxwell A, Sapozhnikov O, Bailey M, Crum LA, Xu Z, Fowlkes B, et al. Disintegration of Tissue Using High Intensity Focused Ultrasound: Two Approaches That Utilize Shock Waves. Acoustics Today. 2012;8(4):24.

2. Khokhlova VA, Fowlkes JB, Roberts WW, Schade GR, Xu Z, Khokhlova TD, et al. Histotripsy methods in mechanical disintegration of tissue: Towards clinical applications. International Journal of Hyperthermia. Informa Healthcare; 2015 Apr 17;31(2):145–62.

3. Pahk KJ, Mohammad GH, Malago M, Saffari N, Dhar DK. A Novel Approach to Ultrasound-Mediated Tissue Decellularization and Intra-Hepatic Cell Delivery in Rats. Ultrasound in Medicine & Biology. 2016 Aug;42(8):1958–67.

4. Carstensen EL. Acoustic cavitation and the safety of diagnostic ultrasound. Ultrasound in Medicine & Biology. 1987 Oct;13(10):597–606.

5. Crum LA. Is Acoustic Cavitation Produced by Diagnostic Ultrasound Devices? IEEE 1987 Ultrasonics Symposium. 1987. pp. 997–1000. Available from: https://doi.org/10.1109/ULTSYM.1987.199108.

6. Barnett SB, Haar Ter GR, Ziskin MC, Nyborg WL, Maeda K, Bang J. Current status of research on biophysical effects of ultrasound. Ultrasound in Medicine & Biology. 1994 Jan;20(3):205–18.

7. Baker ML, Dalrymple GV. Biological Effects of Diagnostic Ultrasound: A Review 1. Radiology. 1978 Feb;126(2):479-83.

8. Xu Z, Ludomirsky A, Eun LY, Hall TL, Tran BC, Fowlkes JB, et al. Controlled ultrasound tissue erosion. IEEE Transactions on Ultrasonics, Ferroelectrics and Frequency Control. IEEE; 2004 Jun 1;51(6):726–36.

9. Xu Z, Fowlkes JB, Rothman ED, Levin AM, Cain CA. Controlled ultrasound tissue erosion: The role of dynamic interaction between insonation and microbubble activity. The Journal of the Acoustical Society of America. Acoustical Society of America; 2005 Jan 1;117(1):424–35.

10. Khokhlova TD, Canney MS, Khokhlova VA, Sapozhnikov OA, Crum LA, Bailey MR. Controlled tissue emulsification produced by high intensity focused ultrasound shock waves and millisecond boiling. The Journal of the Acoustical Society of America. Acoustical Society of America; 2011;130(5):3498–510.

11. Maxwell AD, Khokhlova TD, Schade GR, Wang Y-N, Kreider W, Yuldashev P, et al. Boiling histotripsy: A noninvasive method for mechanical tissue disintegration. The Journal of the Acoustical Society of America. Acoustical Society of America; 2014 Oct 1;136(4):2249–9.

12. Vlaisavljevich E, Kim Y, Owens G, Roberts W, Cain C, Xu Z. Effects of tissue mechanical properties on susceptibility to histotripsy-induced tissue damage. Physics in Medicine and Biology. IOP Publishing; 2014 Jan 20;59(2):253–70.

13. Vlaisavljevich E, Maxwell A, Warnez M, Johnsen E, Cain C, Xu Z. Histotripsy-induced cavitation cloud initiation thresholds in tissues of different mechanical properties. IEEE Transactions on Ultrasonics, Ferroelectrics and Frequency Control. IEEE; 2014 Feb 1;61(2):341–52.

14. Miller DL, Smith NB, Bailey MR, Czarnota GJ, Hynynen K, Makin IRS, et al. Overview of therapeutic ultrasound applications and safety considerations. J Ultrasound Med. American Institute of Ultrasound in Medicine; 2012 Apr;31(4):623–34.

15. Maxwell AD, Cain CA, Hall TL, Fowlkes JB, Xu Z. Probability of Cavitation for Single Ultrasound Pulses Applied to Tissues and Tissue-Mimicking Materials. Ultrasound in Medicine & Biology. 2013 Mar;39(3):449–65.

16. Apfel RE, Holland CK. Gauging the likelihood of cavitation from short-pulse, low-duty cycle diagnostic ultrasound. Ultrasound in Medicine & Biology. 1991;17(2):179–85.

17. Crum LA, Hansen GM. Growth of air bubbles in tissue by rectified diffusion. Physics in Medicine and Biology. IOP Publishing; 1982 Mar 1;27(3):413–7.

18. Kreider W, Maxwell AD, Khokhlova T, Simon JC, Khokhlova VA, Sapozhnikov O, et al. Rectified growth of

histotripsy bubbles. Proc Meet Acoust. ASA; 2013;19(1):075035–5.

19. Coussios CC, Roy RA. Applications of Acoustics and Cavitation to Noninvasive Therapy and Drug Delivery. Annual Review of Fluid Mechanics. Annual Reviews; 2008 Jan;40(1):395–420.

20. Papadopoulou V, Eckersley RJ, Balestra C, Karapantsios TD, Tang M-X. A critical review of physiological bubble formation in hyperbaric decompression. Advances in Colloid and Interface Science. 2013 May;191-192:22–30.

21. Yount DE. A microscopic investigation of bubble formation nuclei. The Journal of the Acoustical Society of America. 1984;76(5):1511.

22. Yount DE. Skins of varying permeability: A stabilization mechanism for gas cavitation nuclei. The Journal of the Acoustical Society of America. Acoustical Society of America; 1979;65(6):1429–39.

23. Blatteau J-E, Souraud J-B, Gempp E, Boussuges A. Gas Nuclei, Their Origin, and Their Role in Bubble Formation. Aerospace Medical Association; 2006 Oct;77(10):1068-76..

24. Brennen CE. Phase Change, Nucleation, and Cavitation. In: Cavitation and Bubble Dynamics. Cambridge: Cambridge University Press; 2009. pp. 1–29.

25. Crum LA. Nucleation and stabilization of microbubbles in liquids. Applied Scientific Research. Kluwer Academic Publishers; 1982;38(1):101–15.

26. Lauterborn W, Kurz T, Geisler R, Schanz D, Lindau O. Acoustic cavitation, bubble dynamics and sonoluminescence. Ultrasonics Sonochemistry. 2007 Apr;14(4):484–91.

27. Lauterborn W, Mettin R. 3 Acoustic cavitation bubble dynamics in high-power ultrasonic fields. In: Power Ultrasonics Applications of High-Intensity Ultrasound. Elsevier; 2015. pp. 37–78.

28. Davitt K, Arvengas A, Caupin F. Water at the cavitation limit: Density of the metastable liquid and size of the critical bubble. EPL (Europhysics Letters). IOP Publishing; 2010 Apr 27;90(1):16002.

29. Vlaisavljevich E, Xu Z, Maxwell A, Mancia L, Zhang X, Lin K-W, et al. Effects of Temperature on the Histotripsy Intrinsic Threshold for Cavitation. IEEE Transactions on Ultrasonics, Ferroelectrics and Frequency Control. IEEE; 2016;PP(99):1–1.

30. Caupin F, Arvengas A, Davitt K, Azouzi MEM, Shmulovich KI, Ramboz C, et al. Exploring water and other liquids at negative pressure. J Phys: Condens Matter. IOP Publishing; 2012 Jul 18;24(28):284110.

31. Kashchiev D. Nucleation. 1st ed. Kashchiev D, editor. Butterworth-Heinemann; 2000.

32. Gallo P, Amann-Winkel K, Angell CA, Anisimov MA, Caupin F, Chakravarty C, et al. Water: A Tale of Two Liquids. Chem Rev. American Chemical Society; 2016 Jul 13;116(13):7463–500.

33. Pahk KJ, Gélat P, Sinden D, Dhar DK, Saffari N. Numerical and Experimental Study of Mechanisms Involved in Boiling Histotripsy. Ultrasound in Medicine & Biology. 2017;43(12):2848-2861.

34. Azouzi MEM, Ramboz C, Lenain JF, Caupin F. A coherent picture of water at extreme negative pressure. Nature Physics. Nature Publishing Group; 2013 Jan 1;9(1):38–41.

35. Caupin F, Herbert E. Cavitation in water: a review. Comptes Rendus Physique. 2006 Nov;7(9-10):1000–17.

36. Debenedetti PG. Metastable Liquids. Princeton Univ; 1991.

37. Vehkamäki H. Classical nucleation theory in multicomponent systems. Classical Nucleation Theory in Multicomponent Systems. Berlin/Heidelberg: Springer-Verlag; 2006. 176 p.

38. Delale CF, Hruby J, Marsik F. Homogeneous bubble nucleation in liquids: The classical theory revisited. The Journal of Chemical Physics. AIP Publishing; 2003 Jan 8;118(2):792–806.

39. Blander M, Katz JL. Bubble nucleation in liquids. AIChE Journal. American Institute of Chemical Engineers; 1975 Sep 1;21(5):833–48.

40. Baidakov VG, Kaverin AM. Boiling-up of superheated liquid argon in an acoustic field. IOP Publishing; 2009 Dec 24;21(46):465103.

41. Baidakov VG. Surface tension of cavitation pockets according to data of computer simulation of nucleation in a stretched fluid. Colloid Journal. Pleiades Publishing; 2015;77(2):119–24.

42. Baidakov VG, Bobrov KS. Spontaneous cavitation in a Lennard-Jones liquid at negative pressures. The Journal of Chemical Physics. AIP Publishing; 2014 May 14;140(18):184506.

43. Schmelzer JWP, Abyzov AS, Baidakov VG. Time of Formation of the First Supercritical Nucleus, Time-lag, and

the Steady-State Nucleation Rate. International Journal of Applied Glass Science [Internet]. 2016 Oct 1;219:1. Available from: http://onlinelibrary.wiley.com/doi/10.1111/ijag.12243/full

44. Herbert E, Balibar S, Caupin F. Cavitation pressure in water. Physical Review E [Internet]. American Physical Society; 2006 Oct 16;74(4):041603. Available from: http://journals.aps.org/pre/abstract/10.1103/PhysRevE.74.041603

45. Fisher JC. The Fracture of Liquids. J Appl Phys [Internet]. 1948;19(11):1062. Available from: http://scitation.aip.org/content/aip/journal/jap/19/11/10.1063/1.1698012

46. Balibar S, Caupin F. Metastable liquids. J Phys: Condens Matter. IOP Publishing; 2002 Dec 13;15(1): S75–S82.

47. Wagner W, Pruß A. The IAPWS formulation 1995 for the thermodynamic properties of ordinary water substance for general and scientific use. AIP Publishing; 2002 Jun 1;31(2):387–535.

48. Bruot N, Caupin F. Curvature Dependence of the Liquid-Vapor Surface Tension beyond the Tolman Approximation. Phys Rev Lett. American Physical Society; 2016 Feb 5;116(5):056102.

49. Menzl G, Gonzalez MA, Geiger P, Caupin F, Abascal JLF, Valeriani C, et al. Molecular mechanism for cavitation in water under tension. 2016 Nov 29, 113 (48) 13582-13587.

50. Oxtoby DW, Evans R. Nonclassical nucleation theory for the gas-liquid transition. Journal of Chemical Physics. 1988 Dec 1;89(12):7521–30.

51. Oxtoby DW. Homogeneous nucleation: theory and experiment. J Phys: Condens Matter [Internet]. 1999 Jan 1;4(38):7627–50. Available from: http://iopscience.iop.org/article/10.1088/0953-8984/4/38/001

52. Vargaftik NB, Volkov BN, Voljak LD. International Tables of the Surface Tension of Water. J Phys Chem Ref Data. AIP Publishing; 1983 Jan 1;12(3):817–20.

53. Schmelzer JWP, Baidakov VG. Comment on "Simple improvements to classical bubble nucleation models". Physical Review E. American Physical Society; 2016 Aug;94(2-2):026801.

54. Baidakov VG. Spontaneous cavitation in a Lennard-Jones liquid: Molecular dynamics simulation and the van der Waals-Cahn-Hilliard gradient theory. Journal of Chemical Physics. AIP Publishing; 2016 Feb 21;144(7):074502.

55. Caupin F. Liquid-vapor interface, cavitation, and the phase diagram of water. Phys Rev E Stat Nonlin Soft Matter Phys. 2005 May;71(5 Pt 1):051605.

56. Cahn JW, Hilliard JE. Free Energy of a Nonuniform System. I. Interfacial Free Energy. 1958 Feb;28(2):258–67. Available from: http://aip.scitation.org/doi/10.1063/1.1744102

57. Kashchiev D. Thermodynamically consistent description of the work to form a nucleus of any size. The Journal of Chemical Physics. 2003;118(4):1837.

58. Briggs LJ. Limiting Negative Pressure of Water. J Appl Phys. 1950;21(7):721.

59. Vlaisavljevich E, Lin K-W, Warnez MT, Singh R, Mancia L, Putnam AJ, et al. Effects of tissue stiffness, ultrasound frequency, and pressure on histotripsy-induced cavitation bubble behavior. Physics in Medicine and Biology. IOP Publishing; 2015 Feb 26;60(6):2271–92.

60. Gonzalez MA, Valeriani C, Caupin F, Abascal JLF. A comprehensive scenario of the thermodynamic anomalies of water using the TIP4P/2005 model. The Journal of Chemical Physics. AIP Publishing LLC; 2016 Aug 7;145(5):054505.

61. Caupin F, Stroock AD. The Stability Limit and other Open Questions on Water at Negative Pressure. In: Liquid Polymorphism [Internet]. Hoboken, NJ, USA: John Wiley & Sons, Inc; 2013. pp. 51–80. (Stanley/Advances Chem Physics V152). Available from: http://doi.wiley.com/10.1002/9781118540350.ch3

62. Vlaisavljevich E, Lin K-W, Maxwell A, Warnez MT, Mancia L, Singh R, et al. Effects of Ultrasound Frequency and Tissue Stiffness on the Histotripsy Intrinsic Threshold for Cavitation. Ultrasound in Medicine & Biology. 2015 Jun;41(6):1651–67.

63. Soneson JE, Ebbini ES. A User-Friendly Software Package for HIFU Simulation. 8TH International Symposium on Therapeutic Ultrasound AIP Conference Proceedings. 2009;1113(1):165-169.

64. Kreider W, Bailey MR, Sapozhnikov OA, Khokhlova VA, Matsumoto Y, Crum LA, et al. The dynamics of histotripsy bubbles. 10th International Symposium on Therapeutic Ultrasound (ISTU 2010) AIP Conference Proceedings. 2011;1359(1):427-430.

65. Pahk KJ, Dhar DK, Malago M, Saffari N. Ultrasonic Histotripsy for Tissue Therapy. Journal of Physics:

Conference Series. IOP Publishing; 2015 Jan 29;581(1):012001.

66. Bailey MR, Khokhlova VA, Sapozhnikov OA, Kargl SG, Crum LA. Physical mechanisms of the therapeutic effect of ultrasound (a review). Acoustical Physics. 2003 Jul;49(4):369–88.

67. Canney MS, Khokhlova VA, Bessonova OV, Bailey MR, Crum LA. Shock-Induced Heating and Millisecond Boiling in Gels and Tissue Due to High Intensity Focused Ultrasound. Ultrasound in Medicine & Biology. 2010 Feb;36(2):250–67.

68. Khokhlova V, Partanen A, Maxwell A, Khokhlova T, Kreider W, Bailey M, et al. Boiling histotripsy method to mechanically fractionate tissue volumes in ex vivo bovine liver using a clinical MR-guided HIFU system. Journal of Therapeutic Ultrasound. 2015;3(Suppl 1): O88.

69. Khokhlova TD, Haider YA, Maxwell AD, Kreider W, Bailey MR, Khokhlova VA. Dependence of Boiling Histotripsy Treatment Efficiency on HIFU Frequency and Focal Pressure Levels. Ultrasound in Medicine & Biology. 2017 Sep 1;43(9):1975–85.

70. Bader KB, Holland CK. Predicting the growth of nanoscale nuclei by histotripsy pulses. Physics in Medicine and Biology. IOP Publishing; 2016 Mar 17;61(7):2947–66.

71. Pahk KJ, Gélat P, Kim, H. and Saffari, N. Bubble dynamics in boiling histotripsy. Ultrasound in Medicine & Biology. 2018;44(12):2676-2696.

72. Haqshenas, S. R., Ford, I. J., Saffari, N., Modelling the effect of acoustic waves on nucleation. The Journal of Chemical Physics. 2016 Jul 14;145(2):024315.

73. Haqshenas, S. R. Modelling the effect of acoustic waves on the thermodynamics and kinetics of crystal nucleation from a solution. Ph.D. thesis, University College London, 2017.